

EMU/bawndc - SM7

ADVANCED RECHNOLOGY DEVELOPMENT
MULTI-COLOR HOLOGRAPHY
(Final Report)

Contract No. NAS8-38609/D.O. 66

Prepared by
Chandra S. Vikram
Center for Applied Optics, The University of Alabama in Huntsville
Huntsville, Alabama 35899

Prepared for
COTR: William K. Witherow
National Aeronautics and Space Administration
George C. Marshall Space Flight Center
Marshall Space Flight Center, Alabama 35812

(NASA-CR-193931) ADVANCED
TECHNOLOGY DEVELOPMENT MULTI-COLOR
HOLOGRAPHY Final Report, 1 Feb.
1993 - 31 Jan. 1994 (Alabama
Univ.) 36 p

N94-27229

Unclas

G3/35 0208988

January 1994

CONTENTS

1. INTRODUCTION	3
2. ERROR ANALYSIS IN THREE-COLOR HOLOGRAPHY	4
3. ALGORITHM FOR PHASE DIFFERENCE MEASUREMENT IN PHASE SHIFTING INTERFEROMETRY	8
4. ROLE OF PHASE DIFFERENCE AMONG COMPONENT HOLOGRAMS ...	12
5. EXPERIMENTS WITH TWO COLOR HOLOGRAPHY	22
6. ANALYSIS OF HOLOGRAMS BY DEFLECTOMETRY	24
7. ANALYSIS BY CONFOCAL OPTICAL PROCESSING	30
8. TEST CELL AND BREADBOARD OPTICAL SYSTEM DESIGN	32
9. CONCLUSIONS	33
REFERENCES	34

1 INTRODUCTION

Holography is an important technique for the materials processing in space program at NASA-George C. Marshall Space Flight Center. The *Fluid Experiment System* (FES) employs holography to monitor several aspects of the fluid in the crystal growth cell. NASA KC-135 as well as *First International Microgravity Laboratory* (IML) employed holography as one of the tools in a reduced gravity environment. *Holographic Optical Laboratory* (HOLOP) and FES are two space qualified holographic systems.

Traditionally, holography is used with one wavelength or color. As such, these holograms provide refractive index information in the crystal growth cell. To extract other quantities (such as temperature and concentration) from this information is not easy and straightforward. Thermocouples can provide the temperature information but they are intrusive and practical at a limited number of places in the cell. In this connection, using two-or more colors for the holography is very important. For example, two colors provide two independent interferograms of the same fluid. The two independent relationships can be used to solve for temperature and concentration variations. Progress in such holography with more than one color is documented.^{1,2}

Another parallel development¹ is possible with non traditional applications of holographic reconstructions. As we know, holography stores and reconstructs the *wavefront*. Traditionally, this wavefront is used for *holography* and *holographic interferometry*. The reconstructed wavefront can in fact be used for a large number of existing and future optical techniques. There are two basic advantages of this approach. First, only one optical system (holographic system) is flown in space, still effectively having the advantage of several hardwares. Secondly, even holograms from a previous space mission can be re-analysed to reveal new information.

In this report, we cover several new aspects of multi-color holography as well as non traditional applications of holographic reconstructions. In particular, the following aspects are covered:

- **Error analysis** in three color holography. This study provides error aspects in three-color holography. The possible advantages and disadvantages of using three-colors are described. A particular three-color combination and a typical triglycine sulfate (TGS) aqueous solution (in the typical crystal growth situation) case is considered in detail.
- **Algorithm** for phase difference measurement in phase shifting interferometry. Phase shifting interferometry is commonly used now for the quantitative analysis of interferograms. In the present study, we have introduced a new algorithm for the phase difference (the quantity actually desired in most applications) analysis. Experiment verification with sugar-water solution is also presented.
- **Role of phase difference** among component holograms. This study provides the role of the

phase difference among different color components in multi-color holography. Fringe intensity variations with some two- and three-color situations are presented and then important conclusions on the fringe contrast are drawn.

- **Experiments** with two color holography. This part covers the progress in two-color holography performed at the Space Science Laboratory at NASA/MSFC in close cooperation with NASA, MetroLaser, and University of Alabama In Huntsville.
- **Analysis of holograms by deflectometry.** This section covers experiments performed using a Ronchi grating and some holograms from Spacelab III mission.
- **Confocal optical processing.** This section covers another application of holographic reconstructions. Again, some Spacelab III holograms were used for this way of analysis.
- **Design** of a breadboard optical system and a test cell. The design and fabrication aspects are summarized here.

2 ERROR ANALYSIS IN THREE-COLOR HOLOGRAPHY

In a previous work, ¹ we reported some aspects of three-color holography. One of the advantages is that we get *three* two-color sets with such an arrangement. Particular advantages are thus the statistical analysis of the data and reconfirmation of the results. Here we present some error aspects. In two color holography, two farthest wavelengths are used so that two linearly independent relationships are obtained to separate two quantities (generally temperature and concentration). In three color holography, another intermediate wavelength is also used. The selection also depends on the available laser wavelengths, system weight, cost, etc. Now the error analysis with each available two-color set must be performed.

In a simple test cell (rectangular parallelepiped), the error $\delta(\Delta T)$ in the temperature change ΔT to be measured is ²

$$\delta(\Delta T) = \pm \frac{\Delta N[\lambda_j |(\partial n/\partial c)_k| + \lambda_k |(\partial n/\partial c)_j|]}{L[(\partial n/\partial c)_k (\partial n/\partial T)_j - (\partial n/\partial c)_j (\partial n/\partial T)_k]} \quad (1)$$

where ΔN is the fractional fringe order measurement capability, L is the longitudinal depth of the test section. $\partial n/\partial T$ and $\partial n/\partial c$ are the gradients of the refractive index (n) against temperature (T) and concentration (c) respectively. j and k represent two-colors and λ is the wavelength.

Also, the error $\delta(\Delta c)$ in the concentration change Δc is ²

$$\delta(\Delta c) = \pm \frac{\Delta N[\lambda_j |(\partial n/\partial T)_k| + \lambda_k |(\partial n/\partial T)_j|]}{L[(\partial n/\partial T)_k(\partial n/\partial c)_j - (\partial n/\partial T)_j(\partial n/\partial c)_k]} \quad (2)$$

Using eqs. (1) and (2), the fractional fringe order accuracy needs (ΔN) can be determined using particular experimental situation. For triglycine sulfate (TGS) aqueous solution (in the typical crystal growth situation), we know ²

$$\partial n/\partial T = -7.6443321 \times 10^{-4} \cdot n(n^2 - 1)/(2n^2 + 1) \text{ } ^\circ\text{C}^{-1} \quad (3)$$

and

$$\partial n/\partial c = 3.16056467 \times 10^{-5} \cdot (n^2 - 1)(n^2 + 2)/n \text{ (gTGS/liter H}_2\text{O)}^{-1} \quad (4)$$

where n is the refractive index whose wavelength λ (in \AA) dependence is given by

$$n = 1.372753 + 366216/\lambda^2 \quad (5)$$

Some results using eq. (3)-(5) are summarized in Table 1. Using a typical $L = 10$ cm, HeNe ($\lambda_j = 632.8$ nm) and HeCd ($\lambda_k = 441.6$ nm) lasers, we obtain

$$\delta(\Delta T) \approx \pm 14 \Delta N \text{ } ^\circ\text{C} \quad (6)$$

and

$$\delta(\Delta C) \approx \pm 33 \Delta N \text{ gTGS/liter H}_2\text{O} \quad (7)$$

respectively. Thus, very accurate fringe orders (small ΔN) measurement capability) is required for small errors or temperature and concentration changes measurement capability.

In three color holography, the errors can be obtained for each of the three two-color sets. One particular example in three-color holography with HeNe ($\lambda = 632.8$ nm), HeCd ($\lambda = 441.6$ nm), and frequency doubled YAG ($\lambda = 532$ nm) lasers. The result of HeNe and HeCd combination is already known by eqs. (6) and (7). For HeNe and frequency doubled YAG lasers, eqs. (3)-(5) or Table 1 can be used in eqs. (1) and (2) to obtain

$$\delta(\Delta T) \approx \pm 38 \Delta N \text{ } ^\circ\text{C} \quad (8)$$

and

$$\delta(\Delta c) \approx \pm 94 \Delta N \text{ gTGS/liter H}_2\text{O} \quad (9)$$

TABLE 1. SOME REFRACTIVE PROPERTIES OF TRIGLYCINE SULFATE
AQUEOUS SOLUTION IN A TYPICAL GROWTH SITUATION AT 45 °C

Laser/Wavelength	Refractive index n	$-\partial n/\partial T$ °C ⁻¹	$\partial n/\partial c$ (gTGS/liter H ₂ O) ⁻¹
HeNe/ 632.8 nm	1.381898	0.00019939	0.000081339
Frequency doubled YAG 532 nm	1.3856914	0.00020137	0.000082272
HeCd/ 441.6 nm	1.391532	0.00020441	0.000083716

Similarly, for the frequency doubled YAG-HeCd lasers combination, we obtain

$$\delta(\Delta T) \approx 20 \Delta N \text{ } ^\circ\text{C} \quad (10)$$

and

$$\delta(\Delta c) \approx 49 \Delta N \text{ gTGS/liter H}_2\text{O} \quad (11)$$

Useful conclusions can be drawn now:

- The need of very accurate fractional fringe order measurement capability ($\Delta N < 1$) remains with each two-color set of this particular three color arrangement.
- Frequency doubled YAG-HeCd laser combination case [eqs. (10) and (11)] demands slightly more accurate fringe counting capability as compared to that with the HeNe-HeCd case [eqs. (6) and (7)].
- HeNe-frequency doubled YAG combination [eqs. (8) and (9)] case demands substantially more accurate fringe counting as compared to the HeNe-HeCd case. Therefore, this case is less desirable for the analysis. Nevertheless, it all depends upon the fringe counting accuracy and required temperature and concentration resolution. For example, if $\Delta N = 1/250$ then $\delta(\Delta T)$ and $\delta(\Delta c)$ of eqs. (8) and (9) become 0.15 °C and 0.36 gTGS/liter H₂O respectively. This may be sufficient in many situations.

The error aspects of this particular three-color holography yields preferable two-color sets for the analysis. However, the methodology is general and can be applied to other laser sources, solution materials, etc.

With the particular three-color case, now we know the minum,intermediate, and maximum errors were for HeNe-HeCd, frequency doubled YAG-HeCd, and HeCd-frequency doubled YAG laser combinations respectively. For the statistical data analysis purpose, all the three results can be combined to reduce the error. Here we present the maximum possible error of such a combination. Let us represent the measured quantity (temperature or concentration) in terms of error and the actual value as

$$\ell_1 = \ell \pm \delta \ell_1 \quad (12)$$

$$\ell_2 = \ell \pm \delta \ell_2 \quad (13)$$

and

$$\ell_3 = \ell \pm \delta \ell_3 \quad (14)$$

where δ -term represents the maximum possible error. Subscripts represents different colors and ℓ is the actual quantity without the error. A weighted average of the quantities can be taken to result in

$$\begin{aligned} \bar{\ell} &= \frac{\ell_1/\delta \ell_1 + \ell_2/\delta \ell_2 + \ell_3/\delta \ell_3}{1/\delta \ell_1 + 1/\delta \ell_2 + 1/\delta \ell_3} \\ &= \ell + \frac{\pm 1 \pm 1 \pm 1}{1/\delta \ell_1 + 1/\delta \ell_2 + 1/\delta \ell_3} \end{aligned} \quad (15)$$

Or, considering the maximum value of the error,

$$\bar{\ell} = \ell \pm 3/(1/\delta \ell_1 + 1/\delta \ell_2 + 1/\delta \ell_3) \quad (16)$$

The maximum possible error $\delta \ell$ is therefore

$$\delta \ell = \pm 3/(1/\delta \ell_1 + 1/\delta \ell_2 + 1/\delta \ell_3) \quad (17)$$

Now we can draw some specific conclusions. The particular TGS aqueous solution case the three temperature measurement maximum errors are $\pm 14 \Delta N^\circ C$ (HeNe -HeCd lasers combination), $\pm 20 \Delta N^\circ C$ (frequency doubled YAG - HeCd lasers combination), and \pm

38 ΔN ° C (HeNe - frequency doubled YAG lasers combination). Using equation (17), the combined maximum error is

$$\delta(\Delta T) = \pm 20 \Delta N \text{ ° C} \quad (18)$$

Similarly, for concentration change, we obtain (using base errors as ± 33 , ± 49 , and ± 94 in gTGS/liter H₂O respectively), we obtain

$$\delta(\Delta c) = \pm 49 \text{ gTGS/liter H}_2\text{O} \quad (19)$$

We see there is no special advantage of using the three two-color combinations from the maximum possible error point of view. However from statistical data point of view, the individual components' errors will not always be maximum, reducing the error. Even so, the individual two color set can be analyzed several times for the statistical data analysis to minimize the error. So, three color holography with three two-color mode of data analysis seems unnecessary. Nevertheless, three color holography appears useful from the following aspects:

- Different wavelengths provide different interference fringe frequencies, providing useful analysis if the frequency is too small or too large with a particular combination.
- Three color lasers, now commercially available, can be used as such without beam combination problems.
- Three unknowns can now be considered to be solved using three interferograms. Thus, one can in principle, eliminate some unwanted effect, such as those due to the window materials, on the interferogram.
- In phase shifting interferometry, several phase measurement errors depend on the phase (or the fringe position) itself.³⁴ With three two-color sets, a particular set can be used at particular spatial location to minimize the error.

Thus, there are several potential uses of three color holography.

3 ALGORITHM FOR PHASE DIFFERENCE MEASUREMENT IN PHASE SHIFTING INTERFEROMETRY

For the quantitative analysis of the interference fringes, here we present a phase shifting algorithm with experimental verification. The method involves only three steps - the original and two equal in amount but unknown phase steps for each stage. Only six frames of data are thus sufficient for the phase difference analysis between two stages. Real time holographic interferometry with concentration change of a sugar-water solution in a test cell is presented for the experimental verification.

Phase measurement interferometry is a well established technique in optical metrology.³⁻⁵ In this, different phase shifts are provided to the original distribution such as an interference pattern. The irradiance data from these shifted patterns are then used to compute the desired phase information. The phase at each point can thus be obtained rather than at fringe maxima or minima in customary interferometry. The whole-field data can be captured by a camera (CCD, CID, etc) and processed by a computer to obtain the phase map over the field. The procedure continues to be refined, critically studied, and applied to new situations.⁶⁻¹⁷

There are several phase measurement algorithms. These are well described by Creath,³ and Greivenkamp and Bruning.⁴ These are *Three Step Method*, *Four Step Method*, *Integrating Method*, *Multi-Step Method*, *Carré Method*, *Hariharan Method*, etc. In one class of methods, the phase steps must be precisely known or calibrated. In the other one, such as in the *Carré Method*, the phase shift need not be known because it is eliminated by the mathematical process of the algorithm. The method is very powerful because it does not need phase calibration and also works with converging or diverging beam where the phase shift varies across the beam.

In the Carré method, the four phase steps are shifted by α to give phase steps of $-3\alpha/2$, $-\alpha/2$, $\alpha/2$, and $3\alpha/2$. The four intensity equations are then solved to yield the unknown phase in the original pattern.

It is interesting to note that in many applications, the phase difference between the two states (or times) of the test field is desired. So determining the absolute phase in the individual pattern is overkill. It is important that the difference measurement may require less number of phase shifts, data storage, simpler phase shifts, etc. We have found one such algorithm that we are reporting here. Like the Carré technique, our method does not need phase calibration. The required phase steps by α are given as $-\alpha$, 0 , and α . The steps are only three (including the original state) and the total phase shift range is reduced from 3α to 2α . Providing linear phase shifts should then be an easier task. The reduced data acquisition should also help the system stability requirements by reducing the total acquisition time.

Let us write the intensity equations for 0 , α , and $-\alpha$ phase shifts as

$$I_1 = A + B \cos \phi, \quad (20)$$

$$I_2 = A + B \cos (\phi + \alpha), \quad (21)$$

and

$$I_3 = A + B \cos (\phi - \alpha), \quad (22)$$

where A and B correspond to the background and the contrast of the pattern and can be space-variant. ϕ is the phase of the original pattern. Now suppose a phase shift δ is

introduced in the original pattern and that is the quantity to be measured. The phase shifts 0 , α , and $-\alpha$ will give the corresponding intensities as

$$I_4 = A + B \cos (\phi + \delta), \quad (23)$$

$$I_5 = A + B \cos (\phi + \delta + \alpha), \quad (24)$$

and

$$I_6 = A + B \cos (\phi + \delta - \alpha). \quad (25)$$

Now the unknown δ can be obtained by the following procedure. First we determine a quantity (say P) as

$$P = \frac{I_6 - I_5}{I_3 - I_2} = \frac{\sin (\phi + \delta)}{\sin \phi} \quad (26)$$

Similarly we determine another quantity (say Q) as

$$Q = \frac{(I_6 - I_4) + (I_5 - I_4)}{(I_2 - I_1) + (I_3 - I_1)} = \frac{\cos (\phi + \delta)}{\cos \phi} \quad (27)$$

Equations (26) and (27) can be solved to obtain

$$\begin{aligned} \cos \delta &= \frac{PQ + 1}{P + Q} \\ &= \frac{(I_6 - I_5)[(I_6 - I_4) + (I_5 - I_4)] + (I_3 - I_2)[(I_2 - I_1) + (I_3 - I_1)]}{(I_6 - I_5)[(I_2 - I_1) + (I_3 - I_1)] + (I_3 - I_2)[(I_6 - I_4) + (I_5 - I_4)]} \end{aligned} \quad (28)$$

The exact value of δ in the complete cycle of 2π can be determined as follows. Equation (28) gives the sign of $\cos \delta$ as such. Assuming the sign of $\cos \alpha$ is known, the relationship

$$I_3 + I_2 - 2I_1 = 2B \cos \phi (\cos \alpha - 1), \quad (29)$$

yields the sign of $\cos \phi$. Then from

$$I_3 - I_2 = 2B \sin \phi \sin \alpha, \quad (30)$$

we obtain the sign of $\sin \phi$. Therefore the sign of $\tan \phi$ or $\cot \phi$ is now known. Finally, from

$$P = \cos \delta + \cot \phi \sin \delta \quad (31)$$

or

$$Q = \cos \delta - \tan \phi \sin \delta \quad (32)$$

the sign of $\sin \delta$ is determined. Once the signs of $\sin \delta$ and $\cos \delta$ are known, we can place the value of δ in the appropriate quadrant.

An interesting aspect of our algorithm is when the phase difference δ is small ($\delta < \pi/2$). Even if the phase terms in the interferograms described by eqs. (20) - (25) cover many cycles (fringes), δ given by eq. (28) will not have phase ambiguities in this situation.

We have performed some preliminary experiments to verify the algorithm. A real-time holographic interferometry set-up to study the phase change of sugar-water solution upon the concentration change was used. First the hologram of a test cell (1 cm inner thickness or the longitudinal path length) containing distilled water was stored. As shown in **Figure**

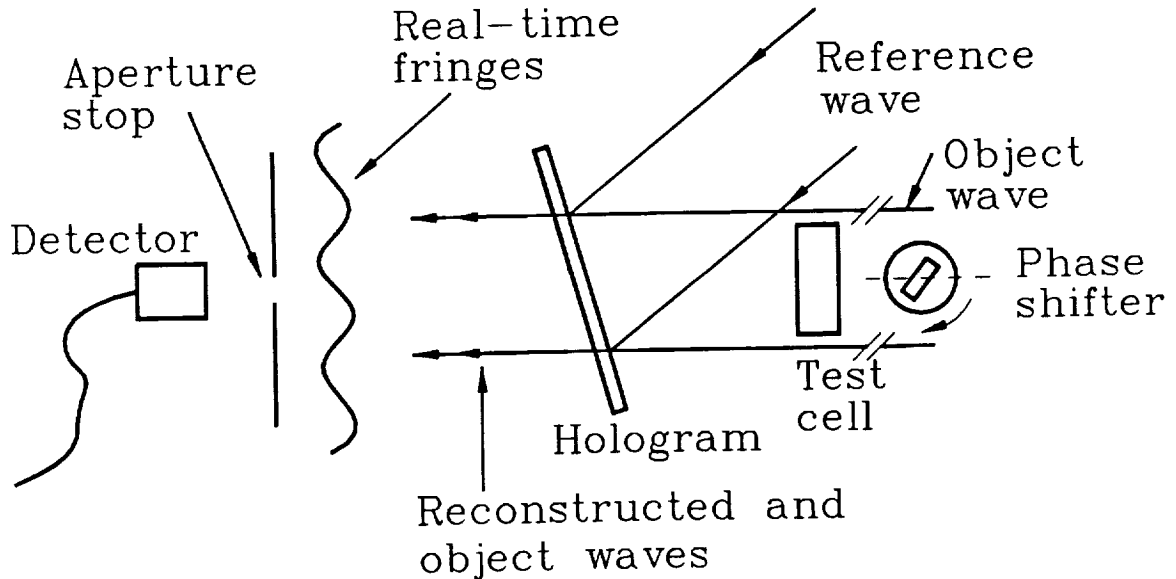


Figure 1. Observation of real-time holographic fringe pattern for the analysis of optical path variations of the fluid in the test cell. HeNe laser of wavelength 632.8 nm was used.

1, the processed hologram was kept back on the original stage to observe real-time fringes.

A photo-detector (much smaller than a fringe) linked to a microvoltmeter was used to measure the intensity. The phase steps were provided by a rotating glass plate (Corning Cover Glass

No. 1½ on a rotation stage) phase shifter.^{3,19} The rotation was provided by a computer controlled translator. Up to 20000 steps of the translator would produce a 2π phase shift. We provided $\alpha = \pi/2$, although this knowledge is not required in our algorithm. However, we will use this later for comparing the results with another algorithm. For the phase change δ , the concentration of the solution was changed by removing some water and replacing by a dilute sugar-water solution. The fact¹⁸ that the refractive index of water at room temperature (20 ° C) changes by 0.00144 for one percent change in the sugar was used. Thus the concentration in the cell was changed to obtain $\lambda/2$ optical path length change (or π phase change, also verified by half fringe shift on the photodetector) for the HeNe laser wavelength $\lambda = 632.8$ nm. The microvoltmeter readings (in μV) I_1, I_2, I_3, I_4, I_5 and I_6 were 352.5, 1015, 255, 781, 68.5 and 911.5 respectively. Equation (20) gives the value of $\cos \delta$ as - 1.0015. This value is very close to the expected value of $\cos \pi = -1$ and proves the general validity of the algorithm. Nevertheless, error analysis and other critical aspects of the technique should follow.

Three step method due to Wyant et al.^{3,20} with $\alpha = \pi/2$ can also be used to determine δ for verification of the results. By replacing our I_1, I_2 and I_3 into their I_2, I_3 , and I_1 respectively, we basically determine $\tan(\phi - \pi/2 - \pi/4)$. Similar data about $\tan(\phi + \delta - \pi/2 - \pi/4)$ can be obtained from our I_4, I_5 and I_6 values. Finally δ can be obtained using $\tan(x - y) = [\tan x - \tan y] / [1 + \tan x \tan y]$. Using our experimental data, we obtain $\tan \delta = 0.037$, or one of the values of δ as 182 °. This value is very close to the expected value.

As we notice, there are five unknowns: A, B, ϕ, δ and α so basically five equations are required to solve for a given quantity. We used six (convenient because we need only three for each set). However solutions using only five equations are possible. For example, using Carré method, we can first solve for A, B, ϕ and α using four initial intensity values. Then using a fifth intensity with an unknown phase difference (δ), δ can be determined. Nevertheless, complicated expressions and additional phase ambiguities are expected.

To conclude, the proposed algorithm for the phase difference measurement requires fewer phase steps (three, as compared to four in the Carré method). The reduction in the total data acquisition time would reduce the system stability time requirements. The phase step range is smaller helping to provide a linear phase change. Thus in a number of situations when the phase difference is the desired quantity we have an alternative option.

4 ROLE OF PHASE DIFFERENCE AMONG COMPONENT HOLOGRAMS

In a previous study,¹ we described the hologram fringe contrast from heterodyning of more than one wavelengths. The general conclusion was that the heterodyning due to the

superimposition of the component holograms reduces the effective hologram fringe contrast in most of the hologram. Consequently, there is no need to have a high customary reference to object beam intensity ratio of the component holograms. The main advantage of reducing the beam intensity ratio is to partly recover the loss of the reconstruction efficiency due to the multiplexing process.

So far we assumed that different holograms due to different colors cover identical paths in the interferometer so that there is no phase difference among them. In the present study, we consider the role of phase difference among them. This phase difference may arise due to different refractive indices (still in the common geometrical path) of different wavelengths passing through window materials, and the phase media itself. More importantly, if there is some advantage from this phase difference, it can be deliberately introduced between two or more holograms. The usual contrast factor $F(\varphi)$ with ideally superimposed holograms¹ is

$$F(\varphi) = \cos \varphi + \cos [(\lambda/\lambda_2)\varphi] + \cos [(\lambda/\lambda_3)\varphi] + \dots \quad (33)$$

where φ is the phase difference between the reference and the object waves at the hologram plane due to the first wavelength λ . $\lambda_2, \lambda_3, \dots$ are the second, third, ... wavelengths respectively.

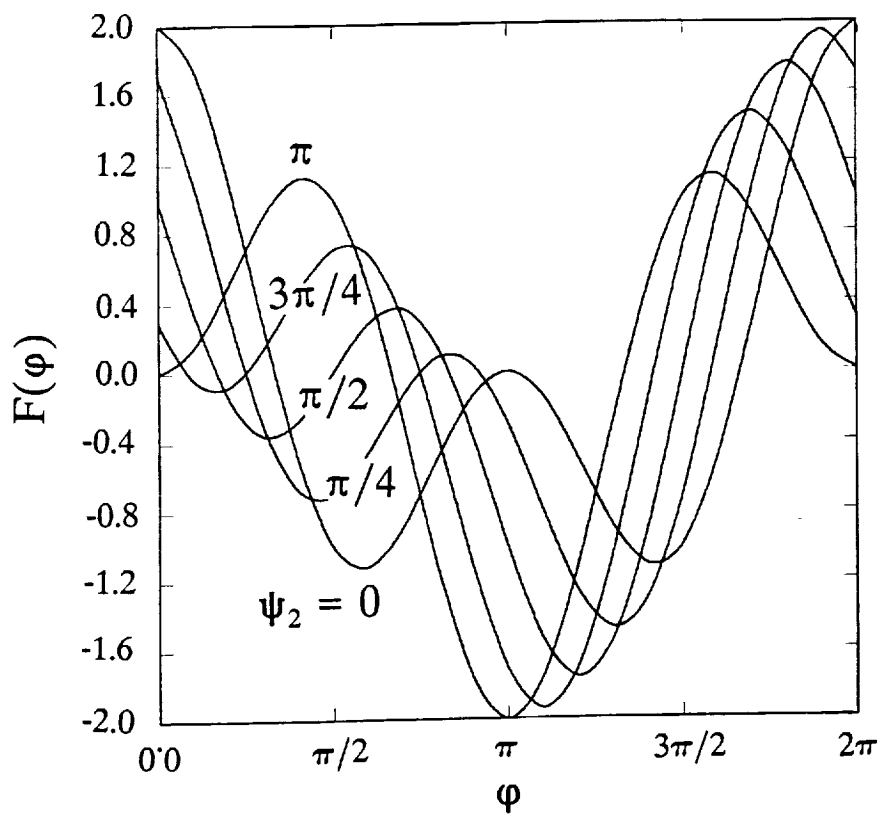
Now ψ_2, ψ_3 , etc. can describe the role of the phase difference among the holograms. These phase factors can be constant as well as space variant. We have already described $F(\varphi)$ without these phase factors for some two- and three-color cases of practical interest. Now we shall describe the role of the additional phase factors.

- *Two color holography with frequency doubled wavelengths.* In this case the function $F(\varphi)$ becomes $\cos \varphi + \cos (2\varphi + \psi_2)$. In **Figure 2**, we have plotted the function $F(\varphi)$ against φ for some values of ψ_2 . As we see that in a complete cycle when ψ_2 changes, maxima and minima both shift up or down in the pattern.

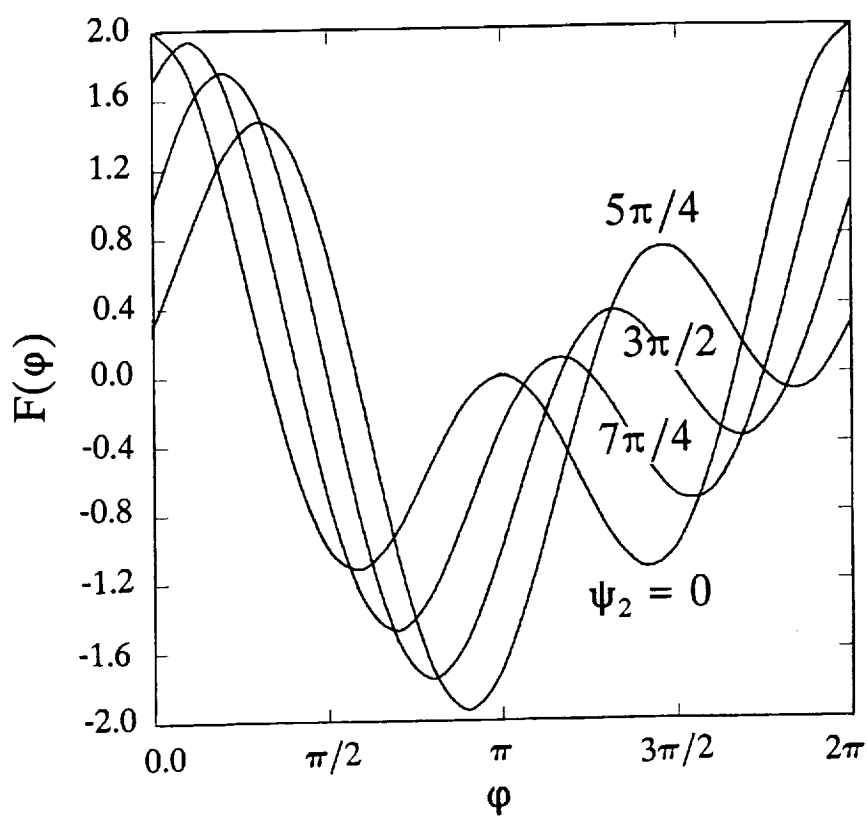
- *Three color holography with HeNe ($\lambda = 632.8 \text{ nm}$), HeCd ($\lambda_2 = 441.6 \text{ nm}$) and frequency doubled YAG ($\lambda_3 = 532 \text{ nm}$).* This is an important practical combination because of the availability of practical laser sources and also about equal wavelength difference between successive wavelengths. In the presence of phase difference among component holograms, we can represent

$$F(\varphi) = \cos \varphi + \cos [(\lambda/\lambda_2)\varphi + \psi_2] + \cos [(\lambda/\lambda_3)\varphi + \psi_3] \quad (34)$$

We have plotted $F(\varphi)$ for this case in **Figure 3**. The solid line corresponds to the usual case^{1,2} without the phase difference whereas the dashed curves are with the respective phase differences. Although we have provided only one phase difference (between only two holograms at a given time) we find considerable differences.

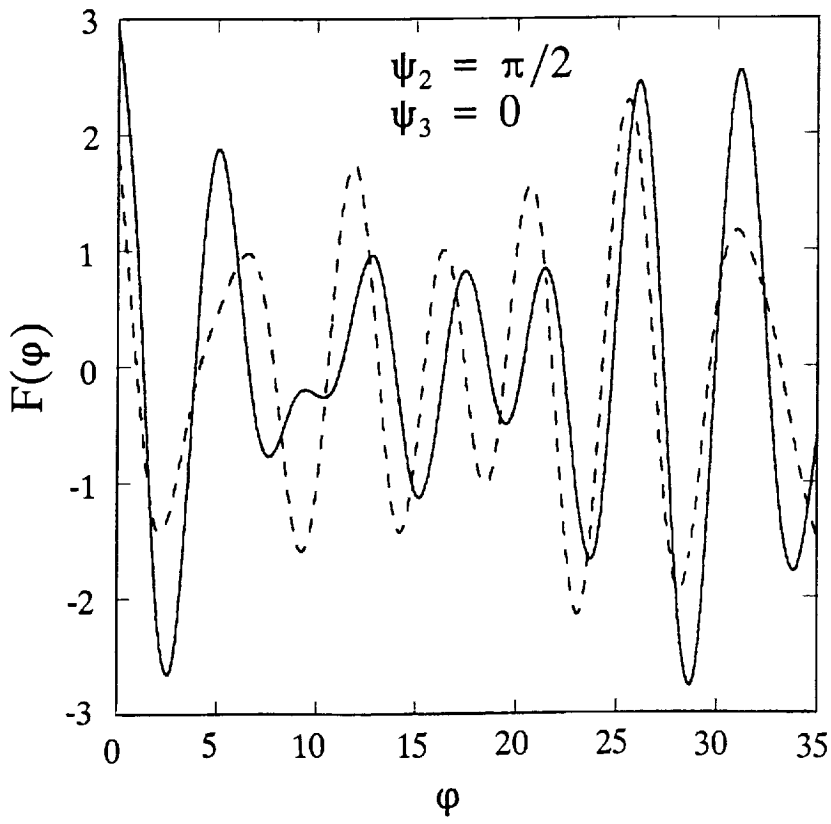


(a)

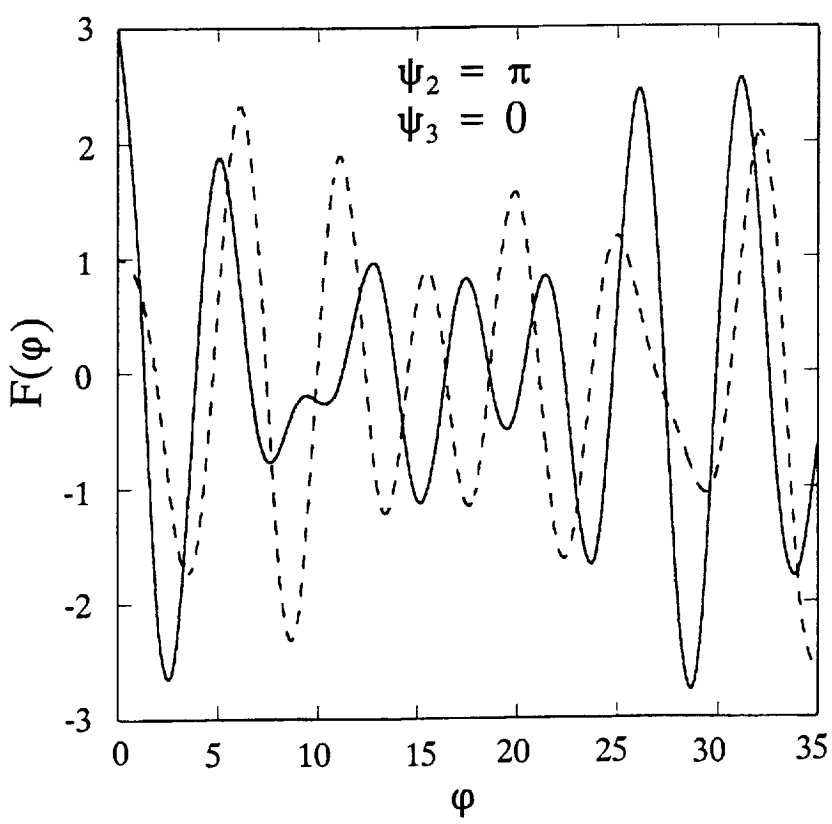


(b)

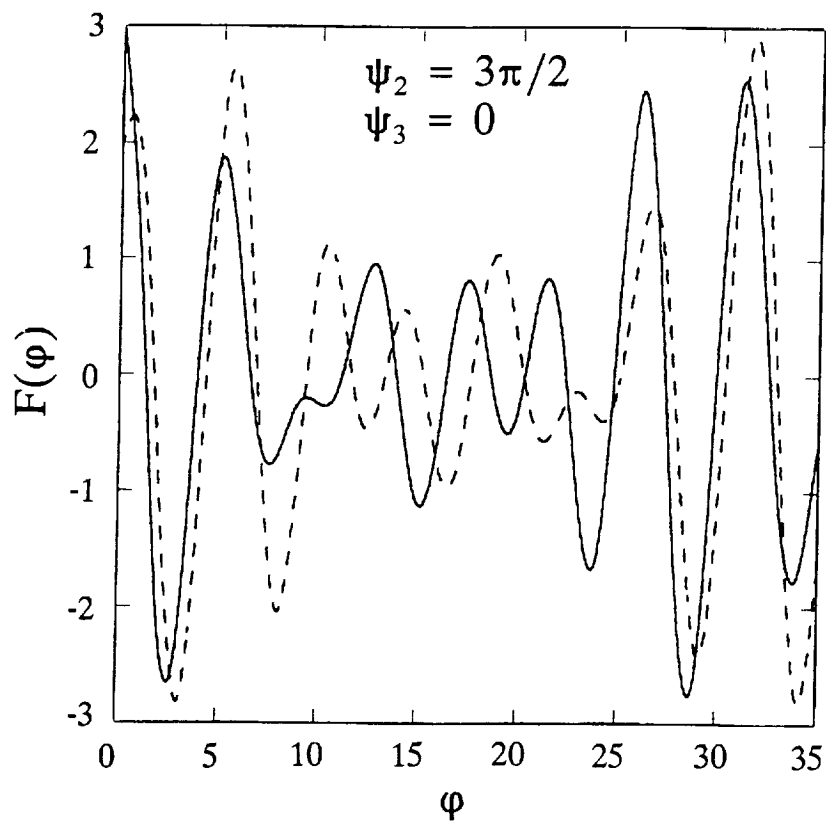
Figure 2. Variation of $F(\phi)$ against ϕ for two color holography with frequency doubled wavelengths. (a) and (b) correspond to different values of ψ_2 .



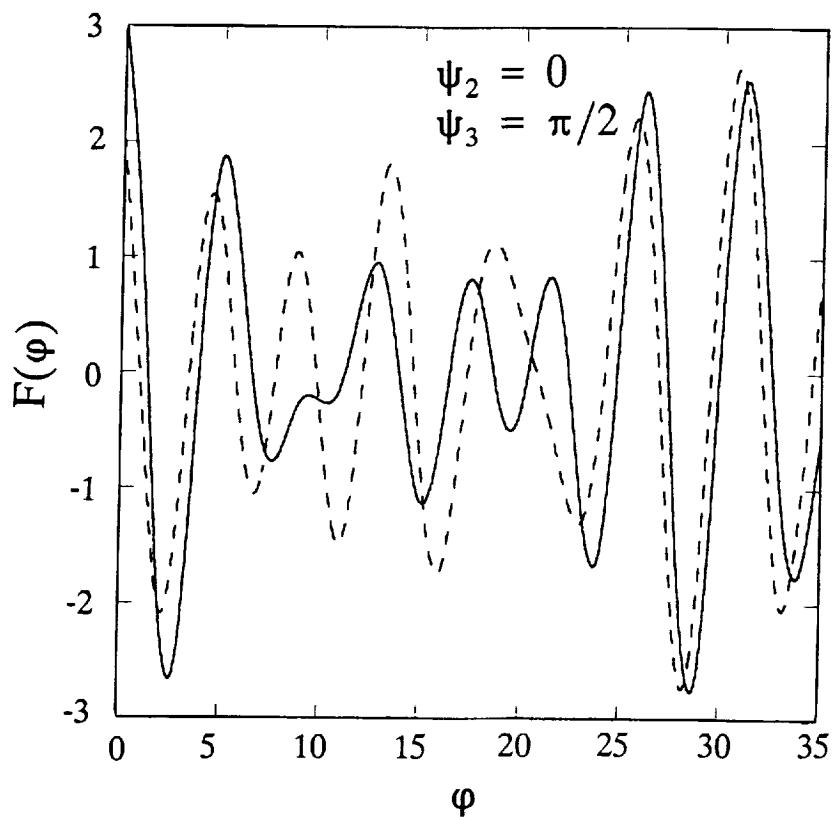
(a)



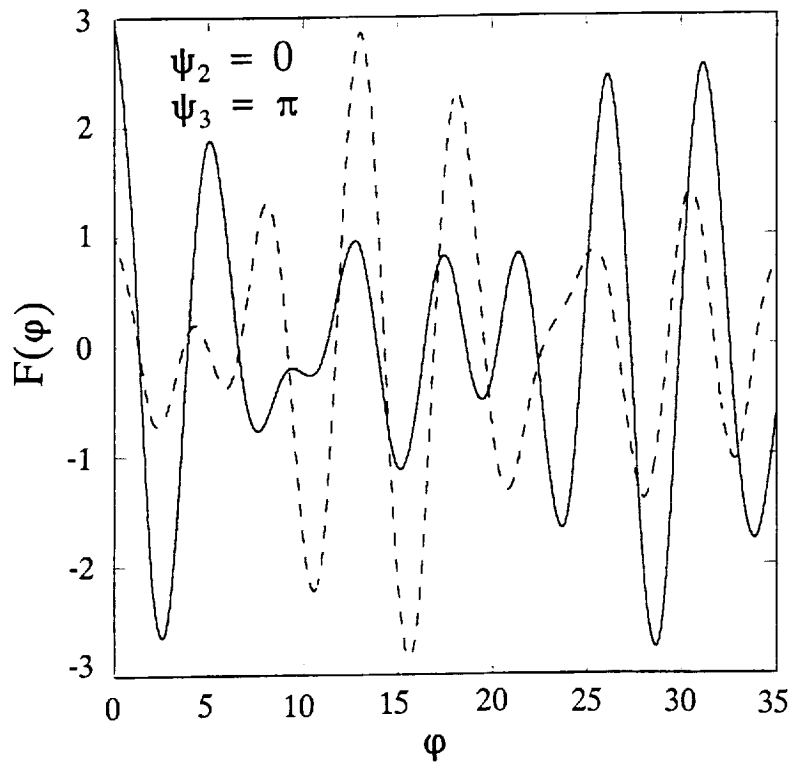
(b)



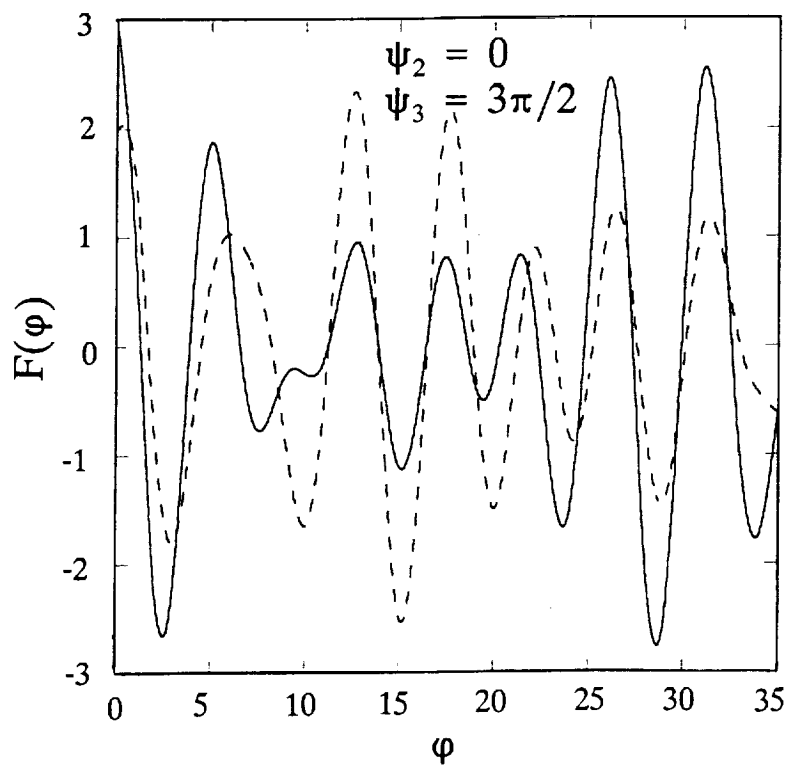
(c)



(d)



(e)



(f)

Figure 3. Variation of $F(\varphi)$ against φ for three color holography with HeNe (wavelength 632.8 nm), HeCd (wavelength 441.6 nm) and frequency doubled YAG (wavelength 532 nm) lasers. (a), (b), (c), (d), (e), and (f) correspond to different values of ψ_2 and ψ_3 , as marked. Solid line corresponds to $\psi_2 = \psi_3 = 0$ in each graph.

In **Figure 3(a)** the maximum difference between the maxima and minima is reduced (as compared to that with the original solid curve). This should be of advantage to have high effective reference to object beam intensity ratio for the entire hologram with a low actual beam intensity ratio. **Figure 3(b)** shows similar trend. In **Figure 3(c)** and **3(d)** the changes are not of any advantage. The results of **Figure 3(e)** and **Figure 3(f)** are interesting. Although the maximum differences between maxima and minima values are generally not reduced by the phases ψ , such maxima and minima are reduced in number. Thus, smaller area of the hologram encounters them. Thus, the phase ψ plays a helpful role in linear hologram recording with a low beam intensity ratio. Therefore, in this case the additional phases ψ are important and have a potential use in the system designing.

Like equation (34) we can represent the general variable part $F(\varphi)$ of the hologram intensity in multi-color holography as

$$F(\varphi) = \cos \varphi + \cos [(\lambda/\lambda_2)\varphi + \psi_2] + \cos[(\lambda/\lambda_3)\varphi + \psi_3] + \dots \quad (35)$$

where λ , λ_2 , λ_3 , etc are the first, second, third, etc. wavelengths. Quantities ψ_2 , ψ_3 , etc. are the mutual hologram phase effects.

In usual single color holography, the factor $F(\varphi)$ varies between + 1 and - 1. With more than one (say N) colors, it will vary between $\pm \beta N$ where $\beta < 1$ is possible in a large portion of the hologram. Some explanation about the coefficient β is appropriate here. We can see from eq. (35) that if N cosine terms are added, the maximum possible values will still vary between $\pm N$. However, due to frequency and phase differences among the cosine terms, destructive interference will occur at different locations of the hologram. The coefficient β is introduced to mathematically describe this situation so that different cases can be compared in the analytical sense. **Figure 3** clearly shows the usefulness of such a coefficient. For example in **Figure 3(a)**, the solid curve covers a large portion with $\beta < 0.6$ (or $F(\varphi) < 1.8$). If just $\cos \varphi$ is plotted, a smaller portion will cover $\beta < 0.6$ [or $F(\varphi) < 0.6$] in the range of the plot. The role of the destructive interference seen for φ between 5 and 25 in **Figure 3(b)** is not there for $N = 1$ case.

Earlier, ¹ we have observed the function $F(\varphi)$ (or β when normalized with N) for some two- and three-color combinations with $\psi_i = 0$. The function varied significantly at least in the limited plotted domain. Also, it was observed that $\beta < 1$ is possible in a large portion of the hologram.

Then earlier in this section we observed significant variations occur due to mutual phase shifts among holograms due to different colors. The variations shown are for a limited number of fringes or only a small portion of a typical hologram. Plots for extended values of φ can be made for further studies. Now we present the results of such a global observation of the situation. Starting with a large number of fringes, we determined the portion of the total hologram area falling within a certain value of β . This is one of the

ways of reaching to some conclusion on the mutual hologram phase effects. As we have found earlier¹ that for a given fringe contrast in the combined multi-color hologram, the standard net ratio (usually between 3 and 10) α and a lower ratio α' of individual holograms, are related by

$$\beta\alpha'^{1/2}/(\alpha' + 1) = \alpha^{1/2}/(\alpha + 1) \quad (36)$$

Thus, the factor β can help visualizing the situation quantitatively. As an example, the lowest possible value of α' ($= 1$) and $\beta = 0.866$ yields the beam ratio α as 3, which is generally sufficient for the linear recording. Now we will see obtainable β values in different situations.

Two- and three-color holography with irrationally related wavelengths

The results of several calculations with these cases are presented here. With the two-color case we considered several combinations, particularly three two-color combinations from HeNe ($\lambda = 632.8$ nm), frequency-double YAG ($\lambda = 532$ nm), and HeCd ($\lambda = 441.6$ nm) lasers. The quantity $|\cos \varphi + \cos [(\lambda/\lambda_2)\varphi + \psi_2]|/2$ was calculated. With each case, the value of φ up to 400π was considered. Calculation was started at $\varphi = 0$ at intervals of 0.01π to the maximum value. Whenever the value of β was less than or equal to a certain assigned value, the particular calculation was counted. In that way the portion of the hologram with β -value less than or equal to a certain number was determined. The calculations were repeated for several values of β . Each calculation was performed for several values of ψ_2 ($0, \pi/4, \pi/2, 3\pi/4, \pi, 5\pi/4, 3\pi/2, \text{ and } 7\pi/4$). It was found that the results were practically independent of the wavelength combination (irrationally related wavelengths in each case) and the phase ψ_2 . This is simple to explain. For a given value of $\cos \varphi$ (say at phase angles $\varphi, 2\pi + \varphi, 4\pi + \varphi, 6\pi + \varphi$, etc.), $\cos [(\lambda/\lambda_2)\varphi + \psi_2]$ will take each possible value between $+1$ and -1 if the wavelength ratio is irrational. Thus at the particular phase of φ the value of the function is independent of the wavelength ratio and the phase ψ_2 . Similar conclusion can be drawn for other values of φ and hence for the entire hologram.

In case of three-color holography, similar calculations were performed for the quantity $|\cos \varphi + \cos [(\lambda/\lambda_2)\varphi + \psi_2] + \cos [(\lambda/\lambda_3)\varphi + \psi_3]|/3$ with several laser wavelength combinations (including the above mentioned wavelengths. Again as expected for the irrationally related wavelengths, the result was independent of the wavelength combination.

The results of these two- and three-color situations are represented in **Figure 4**. The ratio of the hologram portion (less than or equal to certain β -value) to the total hologram has been plotted against β . As we see, for very small values of β , the three-color case has slightly lower ratio as compared to the two-color case. Otherwise, the three-color case generally yields more portion below the certain β -value. As expected the results for both the

cases are common at $\beta = 0$ and 1 points.

Two-color holography with frequency-doubled wavelengths

In this case, the normalized absolute value of the function $F(\varphi)$ becomes $|\cos \varphi + \cos(2\varphi + \psi_2)|/2$. For the portion of the hologram under certain β -value, we calculated the function between 0 and 2π , in intervals of 0.0002π . ψ_2 values considered were 0, $\pi/25$, $2\pi/25$, $3\pi/25, \dots, 2\pi$. The results are plotted in Figure 5. The results are interesting because the role

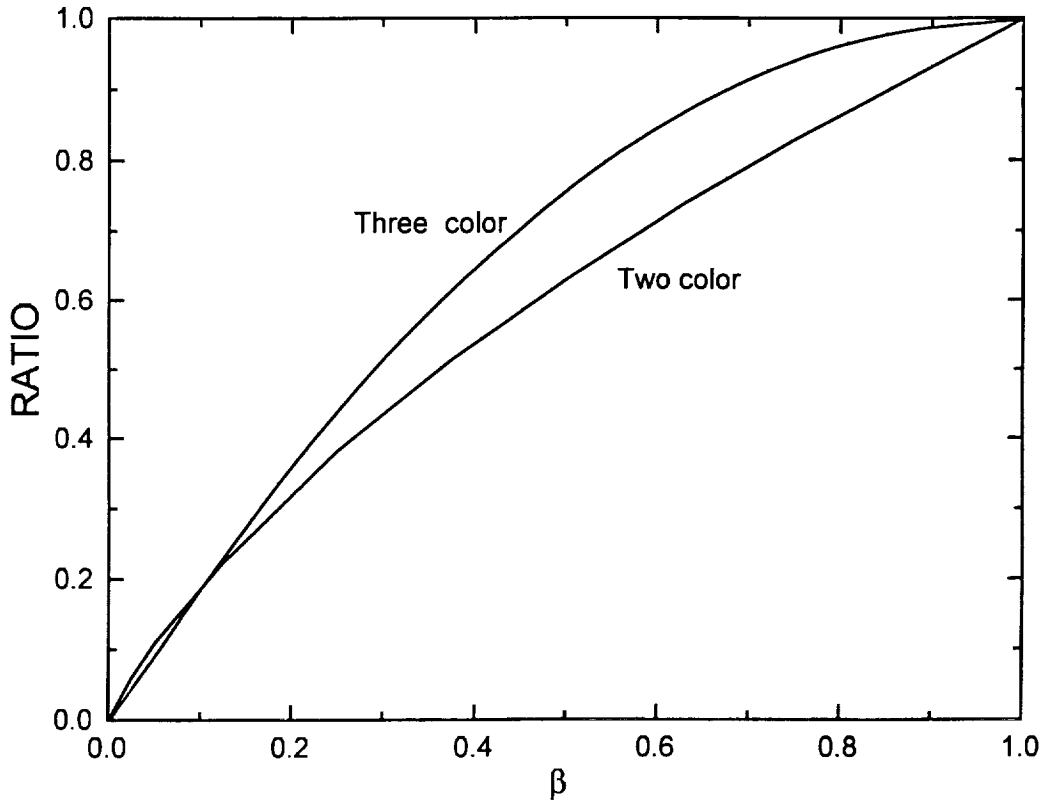


Figure 4. Plot showing the fraction (called ratio) of the hologram equal to or less than certain β -value against β . Irrationally related wavelengths are assumed.

of ψ_2 becomes important. For example, near $\psi_2 = \pi$, the ratio is minimum and maximum depending upon the value of β . Thus, the phase ψ_2 can be an important controlling factor in the system designing.

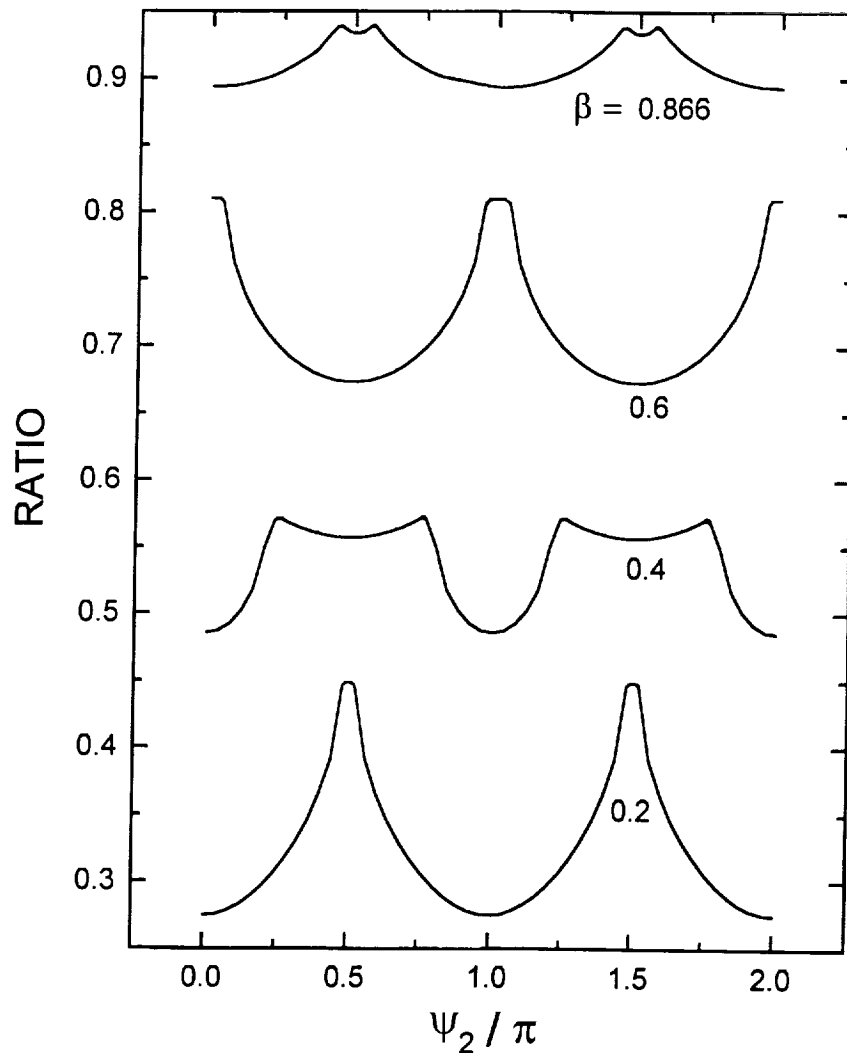


Figure 5. Fraction (ratio) of hologram below a given β -value against ψ_2 . Two-color holography with frequency-doubled wavelengths is considered.

Conclusions on fringe contrast and phase effects in multi-color holography

Mutual phase effects among component holograms in multi-color holography may or may not play a role on the portion of the hologram below a given contrast level. When the wavelength ratios of component holograms are irrationally related, the phase factor does not play a role in the statistical sense. For the rationally related wavelength ratios, the phase factor can play a key role in optimizing the contrast. For two- and three-color holography with irrationally related wavelengths, and two-color holography with frequency-doubled wavelengths, the study has also provided fractions of hologram under different contrast levels.

5 EXPERIMENTS WITH TWO COLOR HOLOGRAPHY

Several experiments have been performed at the Space Science Laboratory at NASA/MSFC in close cooperation with NASA, MetroLaser, and UAH. Initially, the test cell and the control software (by MetroLaser) were tested for their functional performance. Then the system was refined and used for extensive experimentation. Several temperature and/or concentration change experiments of sugar solutions in the test cell were performed. Phase steps were given to store shifted interferograms for the digital data processing. NASA/MSFC is performing data processing, phase unwrapping, etc.

The optical system is represented by **Figure 6**. Basically, the hologram of the test cell containing water is first stored. The processed hologram is kept back on the original stage for real-time observation of the fringes. These fringes are due to the interference between the actual object wave (from the test cell fluid) and the reconstructed image of the cell containing water. The difference between the two times is shown in form of interference fringes. The position of the hologram on the translation stage can be manipulated to obtain a desirable fringe frequency.

The following specific experiments were performed after gaining experiences from the earlier experiments:

- *Real time holographic interferometry with phase shifting.* First, a two-color hologram of the test cell containing water was stored. The processed hologram was replaced back on the original stage to observe real-time interference fringes. Each color (from HeNe or HeCd laser) was used separately to observe the patterns against the changes in the test cell, and the fringe shifter. The experimentation was performed by increasing the temperature on the cell top and bottom to have a minimum temperature somewhat in the middle of the cell section. In another experiment, the concentration at the cell bottom was increased by removing some water and replacing it with a sugar solution, and then increasing the temperature at the top and bottom of the cell. This part was to create a maxima or minima of the temperature and concentration well inside rather than near the wall of the cell. The necessary fringe shifted patterns were digitized by the video camera for further analysis.

- *Holographic storage of the temperature and/or concentration gradients.* This mode of storage is close to the traditional holographic storage in space environment. First, the desired conditions of the test cell were generated and then the hologram (two-color) stored. The reconstructed images were studied in the real-time manner with the test cell now with water without temperature or concentration gradients. There are two main advantages of this approach. First, both the colors are simultaneously used to store the cell condition. Second, this is the traditional NASA method to store the holograms in space. So, there will be minimum changes in the analysis and storage methods, hardware, etc. except replacing the single color laser to a multi-color one. Phase shifted interferograms were stored with temperature minima alone (i.e. just water in the cell) in the middle of the test cell, as well as with a dilute sugar solution at the bottom of the cell and then the temperature condition.

NASA/MSFC performed some data processing of the digitally stored interferograms of these experiments.

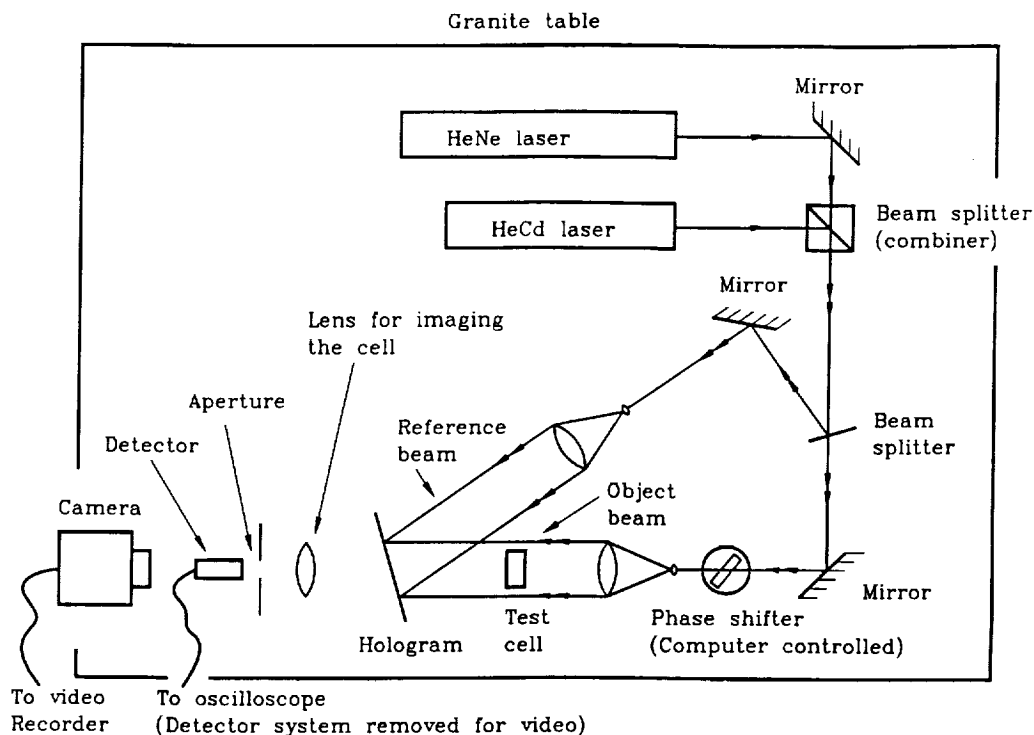


Figure 6. Experimental arrangement for two-color holographic interferometry

Initially we used a photodetector to measure the intensity (of the fringe pattern) at a point. Experiments in Reference 1 as well as in the **Section 3** found usefulness of the method. This procedure was adopted to test the optical arrangement, sensitivity, algorithm, etc. Now we are storing the *whole field* data using a CCD camera so that the processing can be performed using a computer for the entire cross section. We have successfully obtained the phase maps of the entire cross-section and will continue to refine the approach for the ultimate goal of temperature and concentration separation.

The phase shifter is now rotated by a computer controlled translator. The phase shift resolution of $\lambda/10,000$ is available. The test cell temperature (with six thermocouples) is also controlled by the same computer. Details of these computer controlled devices are available elsewhere.²¹

For the data analysis, phase shifting interferometry³⁻⁵ is used. A new algorithm (see **Section 3**) has also been developed.

6 ANALYSIS OF HOLOGRAMS BY DEFLECTOMETRY

Deflection of light passing through a transparent media contains valuable information about the refractive properties of the material processes. For example, Lenski and Braun ²² of Dornier gmbH, Germany used it to study convection in vapor crystal growth experiments. The method is simple from the diagnostics point of view and adaptable to a spaceflight experimentation. We can move one step ahead. A hologram from a mission (say from the NASA FES system) already has the deflection information. Studying the reconstruction in the deflection mode should be possible without any additional hardware as far as the recording is concerned. Also, Lenski and Braun ²³ work uses a single laser beam passing through a region of the test section. Ronchi gratings can also be used ²⁴ for the whole field analysis simultaneously. In our experiments, we have used a Ronchi grating and holograms from Spacelab III mission to establish the approach. Holographic deflectometry was introduced by Verhoeven. ²⁵ However, that method was a pointwise method using an aperture stop. Our approach has the following key features:

- Whole-field analysis by Ronchi grating
- Hologram from an earlier space mission used

The principle of deflection measurement by Ronchi ruling method can be described by **Figure 7**. A collimated light is passed through the deflecting medium (such as a crystal growth test cell). The transmitted light will not remain collimated and the deviation will

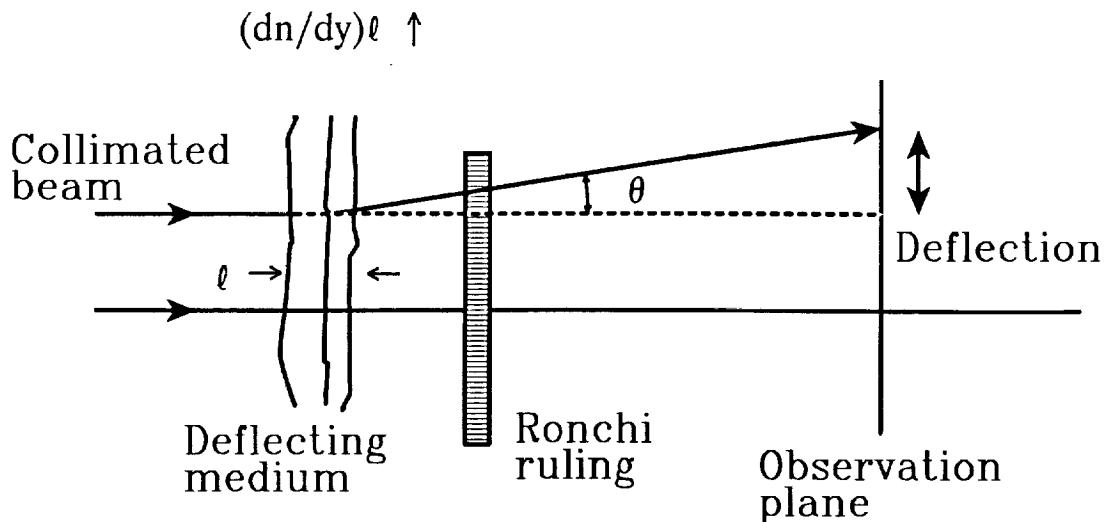


Figure 7. Diagram illustrating deflectometry using a Ronchi grating.

locally vary depending upon the refractive deviations. These ray angles can be measured by placing a Ronchi ruling as shown in the figure. The position of the shadow of the ruling on the observation will reveal the deflection. The angular deflection θ in terms of the mean refractive index gradient dn/dy and the active optical length ℓ is given by ²³

$$\theta = (dn/dy)\ell$$

To adopt the method for holographic reconstructions (such as from an earlier space mission), the principle can be illustrated by **Figure 8**. The hologram of the deflected

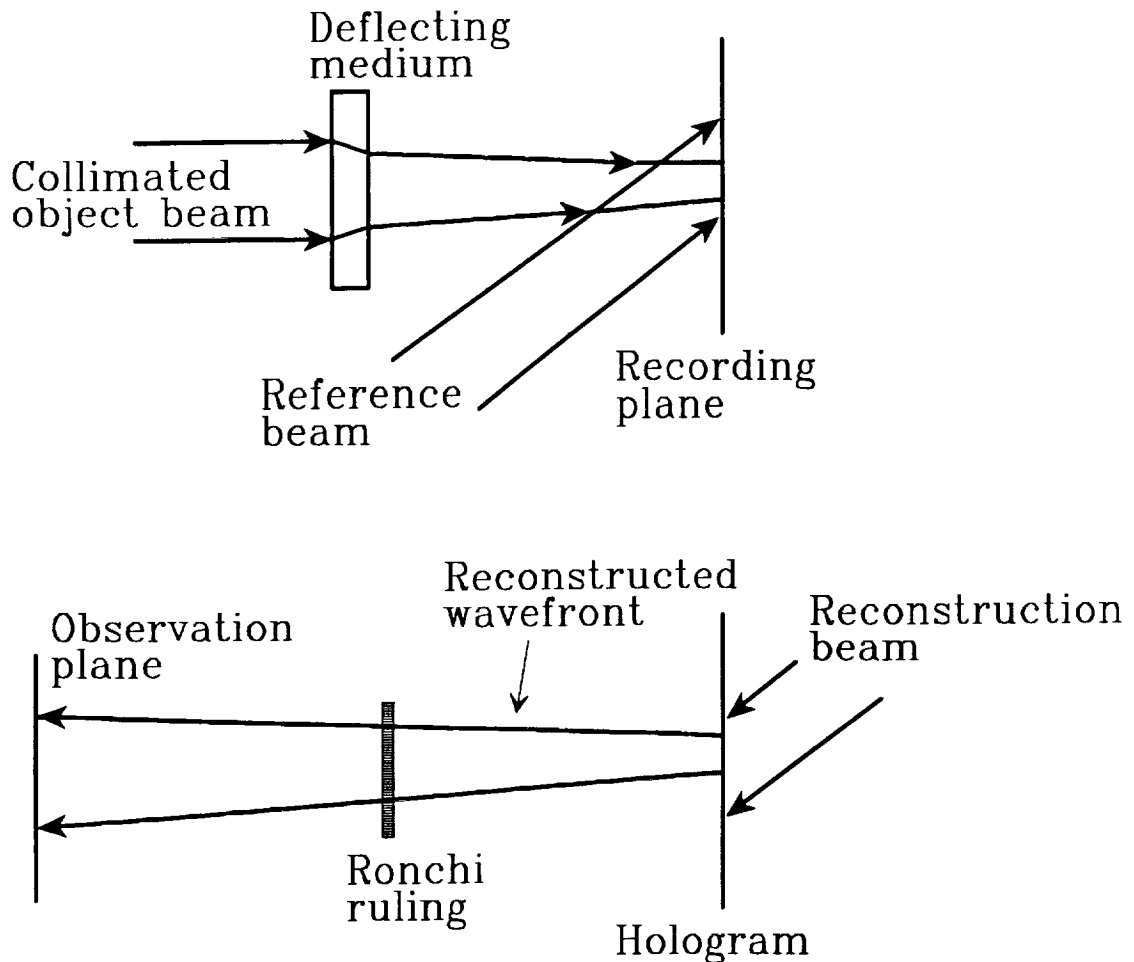
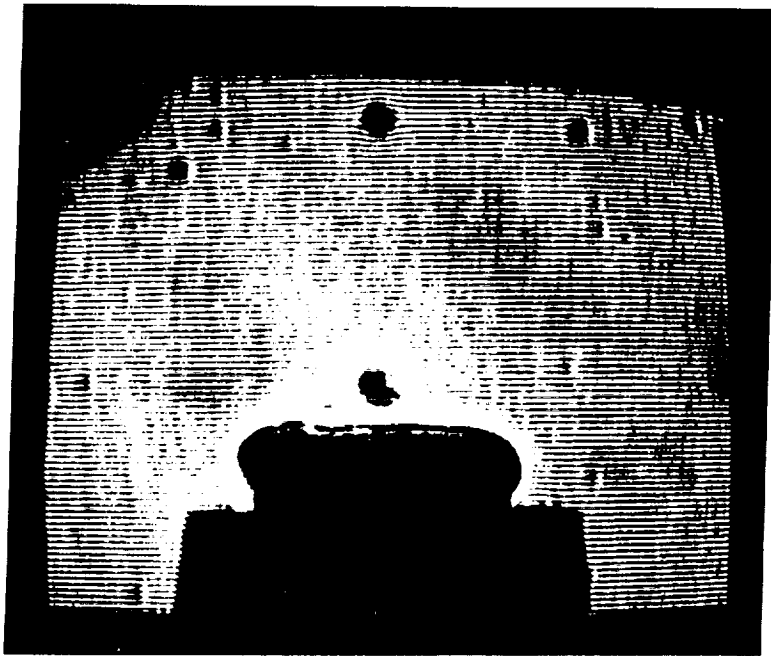
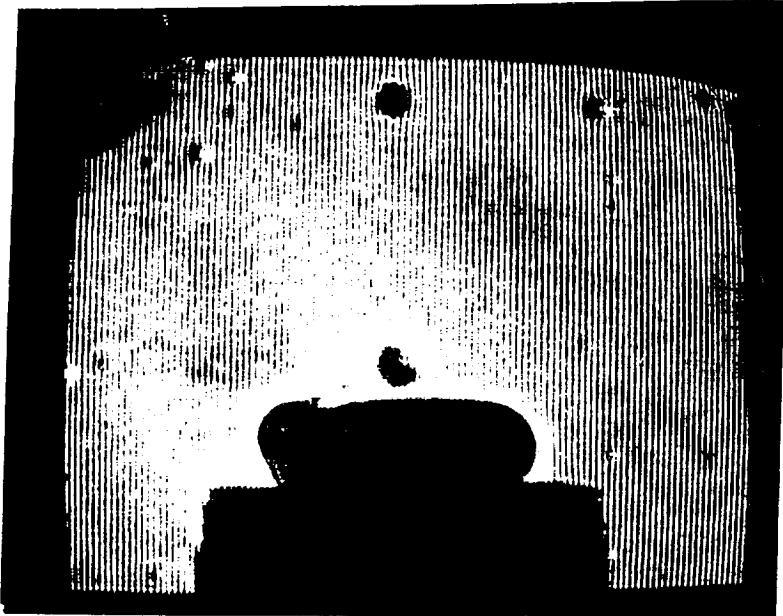


Figure 8. Recording of a hologram of a deflecting medium and subsequent readout of the reconstruction using a Ronchi ruling.

wavefront after passing through the test section is stored. Traditionally, these holograms are reconstructed in the holographic interferometry mode. In the Ronchi ruling approach, the grating can be placed near the real image plane to study the deflection contours. For our experiments, we used a Ronchi grating with 100 line pairs per inch. The holograms were from Spacelab III mission dealing with triglycine sulfate (TGS) crystal growth solution. Results reported here are when the observation plane (ground glass) is 42 cm away from the Ronchi ruling. **Figure 9** correspond to the hologram number 2PO11(14) with horizontal and vertical gratings respectively. This hologram was for a relatively low refractive gradient situation. The lines generally remain unchanged except near the crystal, or when bubbles, etc. are encountered.



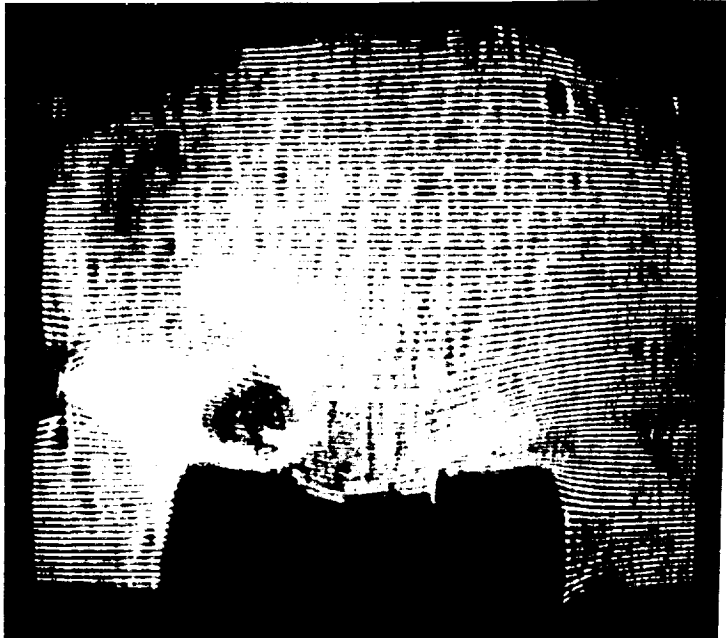
(a)



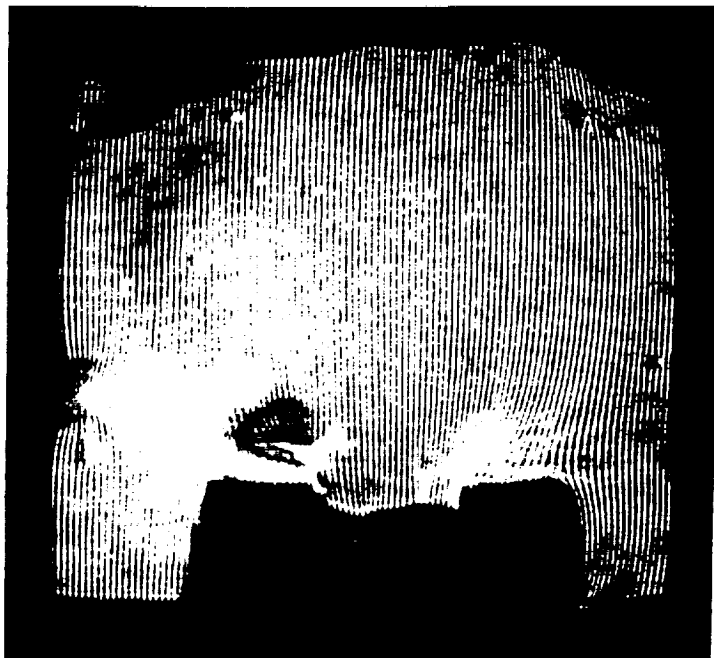
(b)

Figure 9. Observation of the deflected Ronchi gratings from the reconstruction of hologram number 2PO11(14). (a) and (b) correspond to the grating lines horizontal and vertical respectively.

Figure 10 correspond to a relatively higher refractive index gradient situation [hologram number 2PO85(88)]. Not only the higher gradients seen in the form of ruling contours, we see the turbulence effects. From the crystal and upwards, the streams (with local refractive index changes), have different line broadening effects, visualizing these streams. These streams are seen when the lines are horizontal. That means the gradients are dominant in the vertical direction.



(a)



(b)

Figure 10. The deflections from the reconstruction of hologram number 2PO85(88) corresponding to (a) horizontal and (b) vertical gratings.

In **Figure 11**, the hologram [number 2P171(174)] is of a high gradient situation but also contained a grid in the test cell. Those grids, combined by our Ronchi grids, make a complicated pattern, including a Moire pattern. Obviously, as such it is complex for the analysis at this stage.

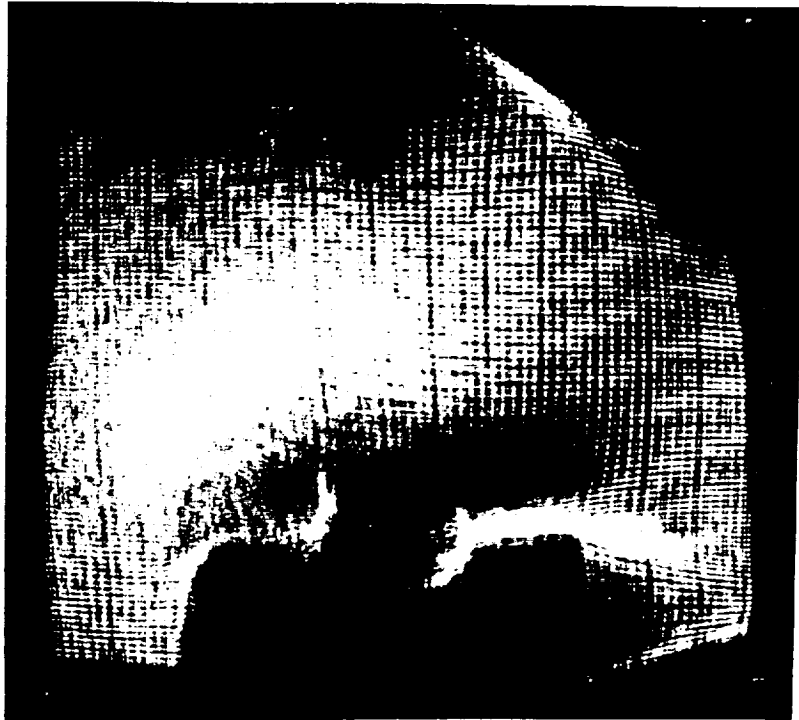


Figure 11. The reconstruction observed by the Ronchi grating in the horizontal direction. The hologram [number 2P171(174)] already contained another grid at the recording stage near the cell.

These early experiments conclude that deflectometry is an useful tool to study holographic reconstructions of large gradients. The approach has the following advantages:

- Whole field approach
- Variable sensitivity by changing the observation plane position.
- No additional instrumental needs for the recording
- Very minimal (such as commercially available Ronchi rulings) additional instrumental needs at the data readout stage.
- The impractical assumption of usual interferometry that there is no ray deflection is not required here.

7 ANALYSIS BY CONFOCAL OPTICAL PROCESSING

In connection to solidification studies, McCay et al. ^{26,27} described the use of confocal optical processing. Basically, this is central dark ground method of the phase contrast to convert refractive index variation into intensity variations. McCay et al. used the system for solidification studies of a simulated metal alloy (ammonium chloride in water). Such optical processing can also be performed from holographic reconstructions, particularly already existing holograms from an earlier space mission. Here we report some results using holograms from Spacelab III mission. As seen in **Figure 12**, the real image is first

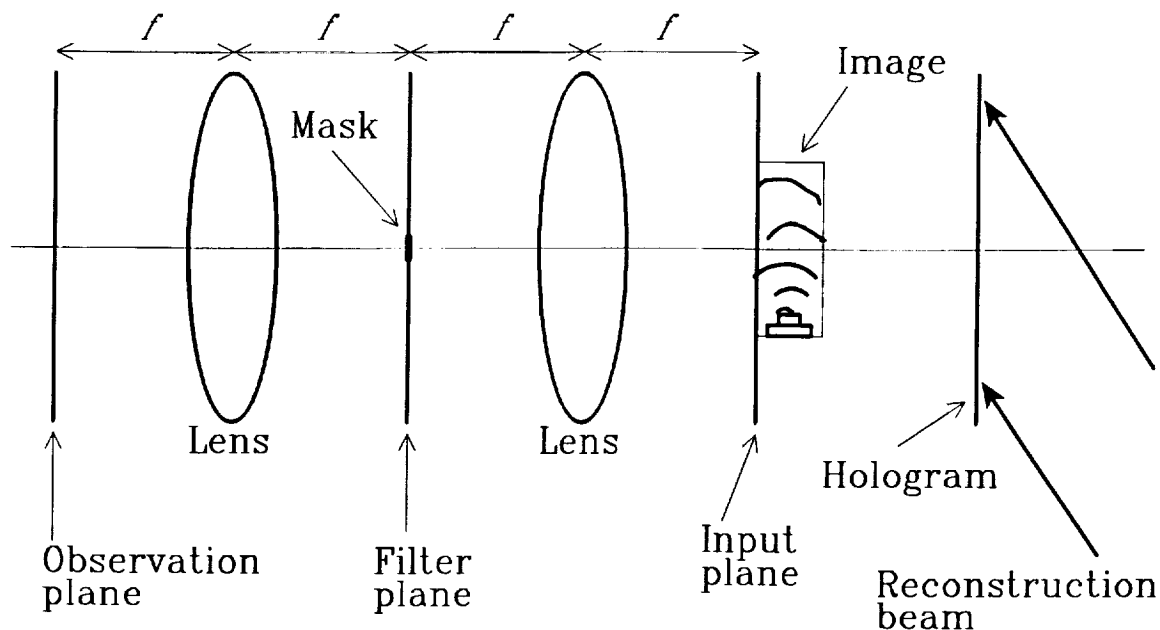


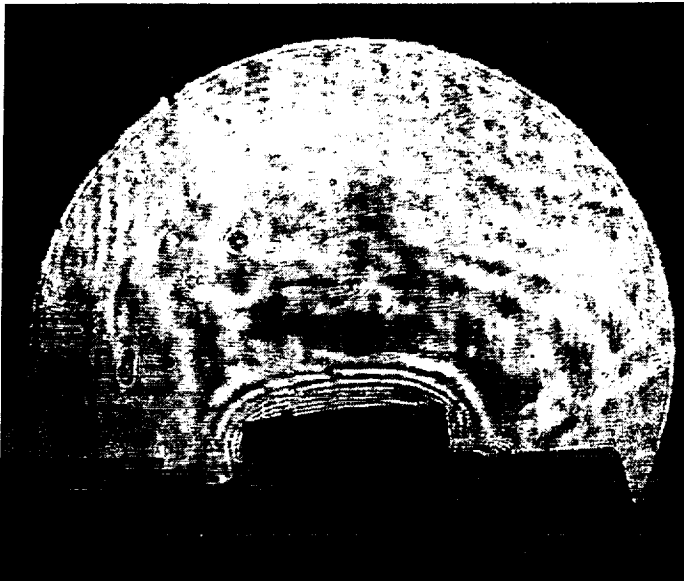
Figure 12. Arrangement for confocal optical processing of the real reconstructed image from a hologram.

reconstructed as usual. A double lens system (each of focal length f) is used to *Fourier Transform* and then *Inverse Fourier Transform* to get the original image back. However, in the Fourier plane, if a small opaque stop is placed to remove some of the low frequency components, then the image intensity will take the form of $A - B \cos \phi$, where ϕ is the phase variation. The fringe like pattern will yield refractive index variations and then ultimately other quantities such as temperature and/or concentration variations. Basically, $\phi(x, y)$ over the cross section is $2\pi/\lambda$ multiplied by the integration of the refractive index variation $n(x, y, z)$ over the thickness τ (in the longitudinal or z -direction) of the test fluid/cell. If there

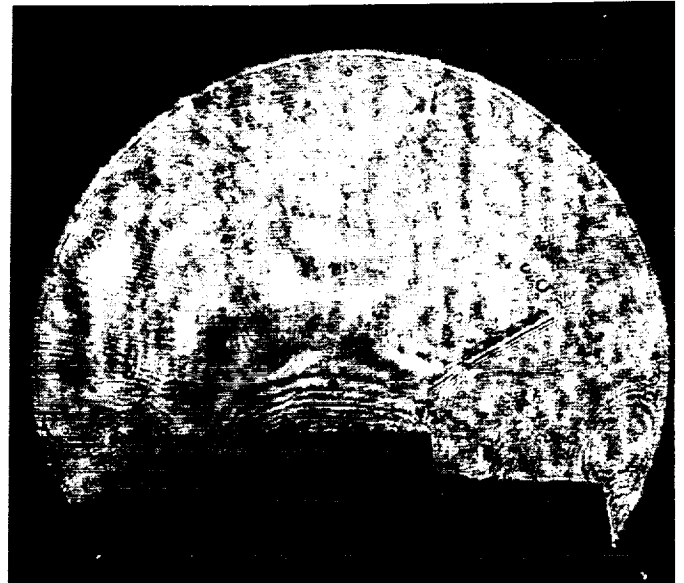
is no index variation in the z -direction, ϕ is simply $2\pi\tau n(x, y)/\lambda$.

In our experiments, holograms from Spacelab III mission were used to reconstruct the images using HeNe laser at 632.8 nm wavelength. The lenses of 16 cm focal length and 4 cm diameter were used. For the spatial filtering, 100 μm square opaque masks on a glass slide was used.

The resulting processed images are shown in **Figure 13**. This was a triglycine sulfate (TGS) crystal growth situation. Obviously, the interference fringes are clearly seen and further analysis for the refractive index can be performed like that in holographic interferometry. As compared to holographic interferometry, the fringe contrast is poorer. Although one may optimize the filter to for the best contrast. On the other hand, the confocal processing method is a quick visualization technique. Also, since both the components for the interference have almost same path, the fringes are very stable. This appears to be a serious advantage of the confocal approach. In usual real-time holographic interferometry, fringe stability is a problem.



(a)



(b)

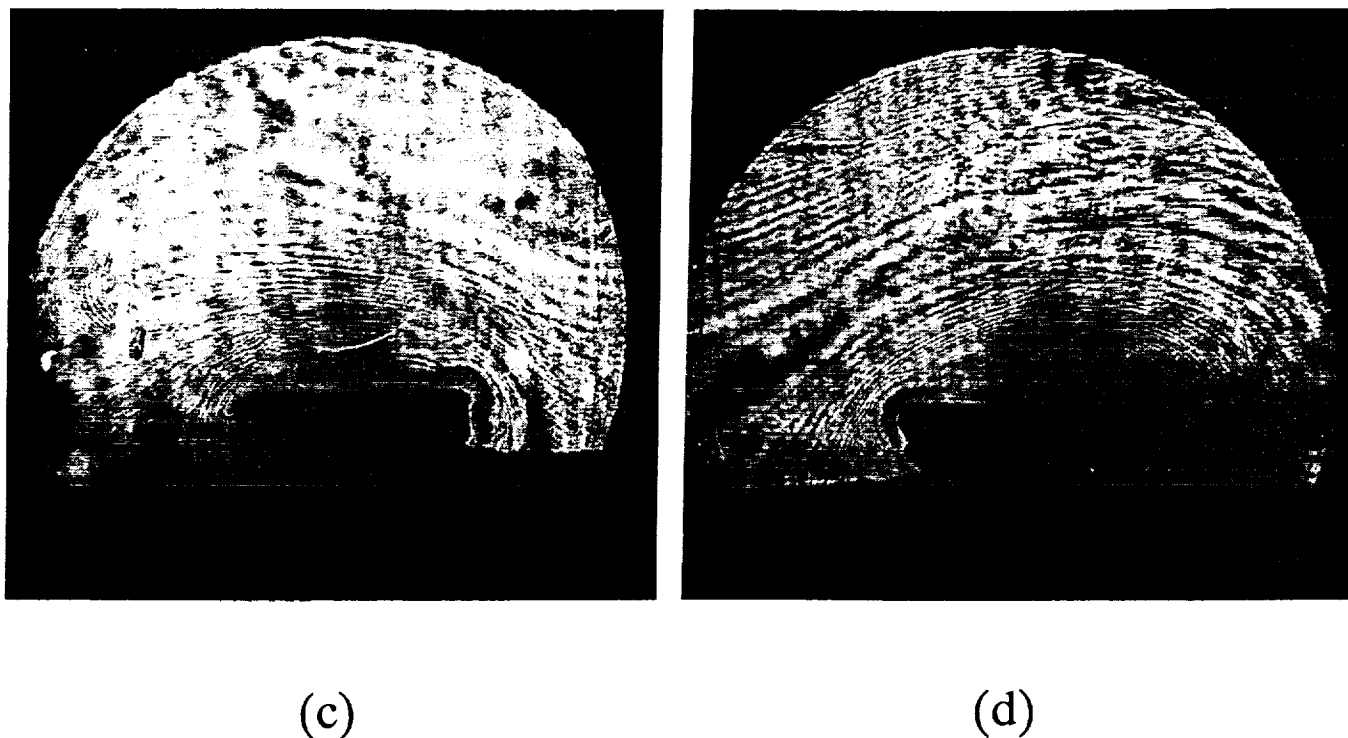


Figure 13. Images obtained by confocal optical processing of some reconstructed wavefronts from Spacelab III holograms. (a), (b), (c), and (d) correspond to hologram numbers 3PO38, 3PO49, 3PO65 and 3PO167 respectively.

8 TEST CELL AND BREADBOARD OPTICAL SYSTEM DESIGN

The designing aspects of the test cell and the breadboard optical system were performed in close cooperation with NASA/MSFC and MetroLaser, California. MetroLaser fabricated these components. The details are reported in the MetroLaser report.²² The important features are summarize here.

The test cell is made of quartz. It is capable of containing a solution of 1 centimeter path length with (i) constant (in space and time), known, adjustable temperature and concentration with the ability to change these quantities, (ii) constant temperature (in space

and time) and a known concentration gradient, and (iii) constant (in space and time) concentration distribution and a known temperature gradient. The ranges and accuracies of these quantities correspond to a typical crystal growth situation. The cell is made of quartz faces with an aluminum cap on the top. To introduce and control temperature and gradients, thermo-electric's are attached above and below of the cell. The cell system is enclosed and mounted in an insulated copper enclosure with open faces of glass windows for the optical access. Thermocouples are mounted at different vertical positions in the cell. The operation and control of the thermal system is done by a computer. For concentration gradients, layers of different solute concentrations can be introduced from the top of the cell using a pipette. Thus, the desired, temperature, concentration, and the gradients can be introduced.

The fiber optic breadboard consists frequency doubled YAG (wavelength 532 nm) and diode (wavelength 680 nm) lasers for two-color holography. Light from each laser is launched into optical fibers. Each color is further divided into two parts (to serve as object and reference beams) using 50/50 beam splitting couplers. For each color, one of the fibers (say the reference) passes through PZT phase controller for the phase shifting. Finally, to combine the beams (due to each color) for holography, the fibers were cemented together. The results of the preliminary experimentation using the system are described in the MetroLaser report. ²²

9 CONCLUSIONS

We have studied several key aspects of multi-color holography including some *non-holographic* mode of analysis of the reconstructed images from holograms. The error analysis in three-color holography helps in suitable selection of wavelengths for the analysis. Also, three color holography has several potential advantages like a range of fringe frequencies for the useful analysis, possible minimization of the error when phase shifting interferometry is used, etc.

The new algorithm developed for the phase difference measurement is unique because it avoids the phase measurement each time and then measuring the difference. The reduction in the total data acquisition time and the system stability time are expected. We have verified the developed theory with experimentation on sugar-water solution.

Another new aspect considered in this study is the role of phase difference among component (individual color) holograms. We have found some interesting results on the effective hologram fringe contrast. Several two- and three-color cases were considered. It is found that the mutual phase effects may or may not play a role on the contrast depending upon the situation. The study should be useful in optimizing the fringe contrast and hence the reconstruction efficiency.

The continued experimentation with two-color holography and phase shifting interferometry are providing the useful data for the digital analysis of the fringe patterns for obtaining the desired refractive index and temperature information. These experiments also helped in

designing and fabrication of a small breadboard system using optical fibers and diode lasers.

Finally, we have successfully demonstrated the use of holographic reconstructions with other (non holographic in nature) analysis mode. This is very important because only hardware is to be flown in space whereas other techniques can be used later on ground at the analysis stage. Even techniques not presently existing can be used with holograms stored on earlier space missions. We have used deflectometry and confocal optical signal processing using Spacelab III holograms. These techniques are very useful from the sensitivity, fringe stability, and other aspects.

In summary, we have been able to push further the state of the art of multi-color holography and unusual applications of holographic reconstructions. Although, crystal growth on earth as well as in microgravity conditions in mind, the study is very general. It should be very useful in holography of heat and mass transfer in general, combustion studied, aero- and fluid-dynamics, etc.

REFERENCES

1. C. S. Vikram, Final Report, *Advanced Technology Development - Multi Color Holography*, Contract No. NAS8-38609/D.O. 30, NASA George C. Marshall Space Flight Center, Huntsville, Alabama, January 1993. See also, C. S. Vikram, W. K. Witherow and J. D. Trolinger, *J. Mod. Opt.* **40**, 1387 (1993).
2. C. S. Vikram, H. J. Caulfield, G. L. Workman, J. D. Trolinger, C. P. Wood, R. L. Clark, A. D. Kathman, and R. M. Ruggiero, Final Report, *Two-Color Holography Concept (T-CHI)*. Contract No. NAS8-38678, NASA George C. Marshall Space Flight Center, Huntsville, Alabama, April 1990.
3. K. Creath, in *Progress in Optics XXVI*, E. Wolf, ed. (Elsevier, Amsterdam, 1988), pp. 349-393.
4. J. E. Greivenkamp and J. H. Bruning, in *Optical Shop Testing, Second Edition*, D. Malacara, ed. (John Wiley, New York, 1992), pp. 501-598.
5. R. S. Sirohi, *Optical Components, Systems, and Measurement Techniques* (Marcell Dekker, New York, 1991), pp. 233-244.
6. P. L. Wizinowich, *Appl. Opt.* **29**, 3271 (1990).
7. K. Creath, *Proc. Soc. Photo-Opt. Instrum. Eng.* **1554B**, 701 (1991).
8. G. Lai and T. Yatagai, *J. Opt. Soc. Am. A* **8**, 822 (1991).

9. K. Creath, Proc. Soc. Photo-Opt. Instrum. Eng. **1553**, 213 (1992).
10. J. van Wingerden, H. J. Frankena, and C. Smorenburg, Appl. Opt. **30**, 2718 (1991).
11. B. Ovryn and E. M. Haacke, Proc. Soc. Photo-Opt. Instrum. Eng. **1553**, 221 (1992).
12. P. K. Rastogi, Appl. Opt. **31**, 1680 (1992).
13. C. Joenathan and B. M. Khorana, Opt. Eng. **31**, 315 (1992).
14. C. Joenathan and B. M. Khorana, J. Mod Opt. **39**, 2075 (1992).
15. T. A. W. M. Lanen and P. G. Bakker, Experiments in Fluids **13**, 56 (1992).
16. Q. R. J. Endo, T. Tanji, and A. Tonomura, Optik **92**, 51 (1992).
17. P. K. Rastogi, Opt. Eng. **32**, 190 (1993).
18. Polarimetry, Saccharimetry of the Sugars, NBS Circular No. 440, 1942, p. 652.
- 19 G. H. Kaufmann and P. Jacquot, Appl. Opt. **29**, 3570 (1990).
20. J. C. Wyant, C. L. Koliopoulos, B. Bhushan, and O. E. George, ASLE Trans. **27**, 101 (1984).
21. J. D. Trolinger, # 4 Technical Report, *Two Color Holographic Interferometry for Microgravity Application*, Contract No. NAS8-39402, DCN: 1-2-ES-44818, NASA Marshall Space Flight Center, Alabama, March 1993.
22. J. D. Trolinger, # 5 Technical Report, *Two Color Holographic Interferometry for Microgravity Application*, Contract No. NAS8-39402, DCN: 1-2-ES-44818, NASA Marshall Space Flight Center, Alabama, November 1993.
23. H. Lenski and M. Braun, Proc. SPIE **1557**, 124 (1991).
24. A. Dahan, G. Ben-Dor and E. Bar-Ziv, Experiments in Fluids **13**, 73 (1992).
25. D. D. Verhoeven, Opt. Communications **74**, 357 (1990).
26. T. D. McCay, M. H. McCay, S. A. Lowry and L. M. Smith, *Convective Effects on Directional Solidification of a Simulated Alloy*, Paper AIAA-88-0258, AIAA 26th Aerospace Sciences Meeting, Reno, Nevada, January 11-14, 1988.
27. M. H. McCay, T. D. McCay and L. M. Smith, Appl. Opt. **29**, 699-703 (1990).



Report Documentation Page

1. Report No. Final		2. Government Accession No.		3. Recipient's Catalog No.	
4. Title and Subtitle Advanced Technology Development Multi Color Holography				5. Report Date 1-19-1994	
				6. Performing Organization Code 5-33157	
7. Author(s) Chandra S. Vikram				8. Performing Organization Report No. Final	
				10. Work Unit No.	
9. Performing Organization Name and Address Center for Applied Optics The University of Alabama in Huntsville Huntsville, Alabama 35899				11. Contract or Grant No. NAS8-38609/D.O.66	
				13. Type of Report and Period Covered Final (2-1-93 to 1-31-94)	
12. Sponsoring Agency Name and Address National Aeronautics and Space Administration Washington, D.C. 20546-001 Marshall Space Flight Center, Alabama 35812				14. Sponsoring Agency Code	
				15. Supplementary Notes	
16. Abstract <p>Several key aspects of multi-color holography and some non-conventional ways to study the holographic reconstructions are considered in this report. The error analysis of three-color holography is considered in detail with particular example of a typical triglycine sulfate crystal growth situation. For the numerical analysis of the fringe patterns, a new algorithm is introduced with experimental verification using sugar-water solution. The role of the phase difference among component holograms is also critically considered with examples of several two- and three-color situations. The status of experimentation on two-color holography and fabrication of a small breadboard system is also reported. Finally, some successful demonstrations of unconventional ways to study holographic reconstructions are described. These methods are <i>deflectometry</i> and <i>confocal optical processing</i> using some Spacelab III holograms.</p>					
17. Key Words (Suggested by Author(s)) Holography, multi-colors, crystal growth, temperature, concentration, space applications, deflectometry, confocal optical processing, breadboard, sugar solution, error analysis, algorithm, phase difference, triglycine sulfate, Spacelab III, Ronchi grating, phase shifting interferometry			18. Distribution Statement		
19. Security Classif. (of this report) Unclassified		20. Security Classif. (of this page) Unclassified		21. No. of pages 36	22. Price